03 Aug 2005

Dynamic Modeling of Slurry Bubble Column Reactors

Novica Rados

Muthanna H. Al-Dahhan
Missouri University of Science and Technology, aldahhanm@mst.edu

Milorad P. Duduković

Recommended Citation

N. Rados et al., "Dynamic Modeling of Slurry Bubble Column Reactors," *Industrial and Engineering Chemistry Research*, vol. 44, no. 16, pp. 6086 - 6094, American Chemical Society, Aug 2005.
The definitive version is available at https://doi.org/10.1021/ie040227t

Dynamic Modeling of Slurry Bubble Column Reactors

Novica Rados,† Muthanna H. Al-Dahhan,* and Milorad P. Duduković

Chemical Reaction Engineering Laboratory, Washington University in St. Louis, Campus Box 1198, One Brookings Drive, St. Louis, Missouri 63130-3899

The multicomponent, one-dimensional, and compartment-based dynamic model developed by Rados et al. (*Catal. Today* **2003**, *79*−*80*, 211−218) has been used to study the performance of slurry bubble columns operated with two chemical reaction systems. One reaction causes contraction in the gas-phase volume, and the other causes expansion. The change in the gas flow rate (expansion or contraction) along the reactor as a result of the chemical reaction kinetics is accounted for by the overall mass balance of the gas phase represented by large and small bubbles. The importance of properly accounting for the change in the gas flow rate has been demonstrated. The backmixing in the three compartments of the model (small bubbles, large bubbles, and slurry) is accounted for by the axial dispersion model. The effects of operating conditions and reactor dimensions on the slurry bubble column performance have been evaluated. A detailed analysis of the role of backmixing on the performance of the Fischer−Tropsch synthesis (contraction of the gas phase) has been conducted by varying the axial dispersion coefficient (E) of the three phases between ideal plug flow (E = 0) and completely mixed flow (E = ∞).

1. Introduction

Slurry bubble column (SBC) reactors are the reactors of choice for various processes in the chemical and biochemical industries [oxidation, hydrogenation, chlorination, alkylation, polymerization, and methanol and Fischer−Tropsch (FT) synthesis].[1−3] SBCs are cylindrical vessels in which gas reactants are sparged through a slurry of small catalyst particles in a mixture of liquid products, dissolved reactants, and often inert substances. Despite their simple construction, their design and scale-up are still quite uncertain because of the not yet fully understood complex interaction among the phases (gas, liquid, and solids).

SBC reactors offer several advantages, such as nearly isothermal operation, good interphase contacting, large catalyst area, good productivity, operational flexibility, low pressure drop, and low construction and operational costs. However, disadvantages of the slurry reactors are significant backmixing, difficult separation of solids and liquid, and uncertain scale-up. Because their advantages often overcome the disadvantages, SBCs are the preferred type of reactor for numerous processes, particularly highly exothermic ones, when efficient interphase contacting is needed and when significant phase backmixing is not detrimental to the operation.

In three-phase gas−liquid−solids (G−L−S) slurry systems, the suspension of solids in liquid is usually modeled as a single pseudo-homogeneous slurry phase (SL). Within the slurry phase, the solids velocity is assumed to be equal to the liquid velocity. Hence, SBC reactors are most often modeled as two-phase gas−slurry (G−SL) systems. Given the fairly small size of the solid particles that are typically used in SBC reactors (mean size below 50 μm), the pseudo slurry assumption is probably reasonable.

Most of the models assume a uniform concentration of the solids throughout the reactor. Following the work of Kato et al.,[4] some models calculate the solids axial concentration profile using the sedimentation and dispersion model (SDM)[5,6] or the mechanistic model.[7] These models have shown that, despite the small size of the solids, the axial profile of the solids concentration in the slurry may not be flat. The shape of the axial profile strongly depends on the slurry system properties and the operating conditions. In batch slurry operation, the catalyst concentration is highest at the bottom of the column and exponentially decreases with height. Catalyst axial profiles in the co- and countercurrent modes of operation strongly depend on the direction and magnitude of the slurry inlet velocity.[6]

Large-scale SBC reactors operate either in the bubbly (homogeneous) flow regime or in the churn-turbulent (heterogeneous) flow regime. In the bubbly flow regime, the gas phase is usually modeled as a single phase consisting of uniform size bubbles.[8,9] However, in churn-turbulent flow, a full spectrum of different bubble sizes and shapes exists. On the basis of experimental observations and measurements in the churn-turbulent regime, the bubble population has been divided into two broad classes: large and small bubbles.[10,11] Large bubbles rise straight up through the column without recirculation. Because of their lower rise velocity, small bubbles circulate within the column before eventually disengaging at the top.

The two-bubble-class approach has been used by Maretto and Krishna,[12] van der Laan et al.,[13] and de Swart[14] in modeling the FT SBC. Cross-flow (CF) interaction between the small and large bubbles either is neglected[15] or is modeled as infinite, forcing the same composition in both bubble classes.[16] Both of these approaches are limiting cases, whereas the physical extent of interaction between small (SB) and large bubble (LB) phases would be somewhere in between.

Backmixing within the phases either has been modeled as infinite (complete mixing, i.e., continuous stirred

* To whom correspondence should be addressed. Tel.: +1 (314) 935-7187. Fax: +1 (314) 935-4832. E-mail: muthanna@seas.wustl.edu.

† Current address: ExxonMobil Research and Engineering, 3225 Gallows Road, Room 8A 1730, Fairfax, VA 22037-0001.

10.1021/ie040227t CCC: $30.25
Published on Web 06/11/2005

tank, CST, representation) or has been completely neglected (plug-flow, PF, representation). Because the majority of industrial reactors operate with a finite amount of backmixing, nonideal flow models that account for the finite amount of phase backmixing are more appropriate for modeling of real reactor systems. These models fall into two broad groups: axial dispersion models (ADMs)[6,16,17] or multicell models (MCMs).[18−21] The MCM model was found to be computationally much faster and numerically more stable than the ADM model, particularly in the case of steep solution profiles.

However, most of the published SBC models are for steady-state operation. The dynamics of process transitions (start-up, shutdown, and change in the set points) are extremely complex and in industry are dealt with by heuristics rather than reliable simulation predictions. Therefore, there is a large need for dynamic models that can accurately model process transitions. In 2002, de Swart and Krishna[22] proposed a simplified dynamic slurry reactor-scale model. The model assumes a linear relationship between the gas flow rate and the conversion, which represents a limitation in its application. Additionally, their model does not account for the CF exchange of mass that is caused by the interactions between small and large bubbles.

Many chemical processes operate with a change in the gas flow rate due to chemical reaction kinetics that involves uneven numbers of reacted and produced moles. Hence, to capture the effect of such conditions, a proper reactor-scale model should account for the change in the gas flow rate and consequently the change in the gas holdup.[23,24] This need makes the model numerically involved and difficult to solve. Most of the reactor-scale models that account for the change in the gas flow rate employ a simplified approach based on the linear relationship between the gas flow rate and the conversion.[25] This approach can be applied only in some limited cases.[24] However, in most real industrial situations, such as FT synthesis, a more realistic approach is needed. Accordingly, Rados et al.[26] developed a multicomponent, one-dimensional dynamic model for churn-turbulent flow in SBC reactors where the change in the gas flow rate due to the chemical reaction was modeled using the overall gas mass balance. They utilized the model to simulate FT synthesis in a SBC where the gas phase chemically reacts and is reduced in volume and flow. In this model, all of the variables, including the gas velocity and gas holdup, are treated as time- and space-dependent. This is unlike some of the existing models that linearize the change in the gas velocity and/or the gas holdup in space and time,[6,22] where the gas velocity and/or the gas holdup are algebraically calculated and updated between numerical steps.

In the present work, the dynamic model developed by Rados et al.[26] has been utilized to study and compare the performances of different SBC reactors operated with expansion or contraction in the gas flow. Furthermore, analysis of the role of backmixing on the FT synthesis performance is presented.

2. General Form of the Rados et al.[26] Model

Rados et al.[26] divided the SBC flow structure into three compartments (Figure 1), where each compartment represents one of the three modeled phases: SB, LB, and SL phases. Mass transfer between liquid and gas phases is included. Interactions between SB and LB

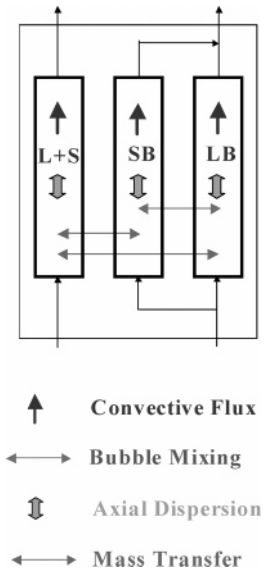

Figure 1. Schematic representation of the SBC reactor model.

are accounted for by the CF mass exchange. The magnitude of these interactions is assumed to be finite and directly proportional to the slip velocity between the two gas phases (SB and LB). Axial dispersion is considered in all of the three phases. In the gas phases, the axial dispersion is caused by the interactions among bubbles of the same class. In the liquid−slurry phase, the axial dispersion is related to the liquid−slurry phase backmixing. In the work by Rados et al.,[26] the model was presented in dimensionless forms. Hence, for usefulness and completeness of the reported model structure, the dimensional forms of the model are given here.

The species mass balance in SB is expressed as follows:

$$\frac{\partial(\epsilon_{SB}C_{SB,j})}{\partial t}+\frac{\partial(U_{SB}C_{SB,j})}{\partial z}=-(U_{LB}-U_{SB})\frac{K}{H_D}(C_{SB,j}-C_{LB,j})-(k_La)_{SB,j}\left(\frac{C_{SB,j}}{He_j}-C_{L,j}\right)+\frac{\partial}{\partial z}\left(\epsilon_{SB}E_{SB}\frac{\partial C_{SB,j}}{\partial z}\right) \quad (1)$$

The species mass balance in LB is expressed similarly:

$$\frac{\partial(\epsilon_{LB}C_{LB,j})}{\partial t}+\frac{\partial(U_{LB}C_{LB,j})}{\partial z}=-(U_{LB}-U_{SB})\frac{K}{H_D}(C_{LB,j}-C_{SB,j})-(k_La)_{LB,j}\left(\frac{C_{LB,j}}{He_j}-C_{L,j}\right)+\frac{\partial}{\partial z}\left(\epsilon_{LB}E_{LB}\frac{\partial C_{LB,j}}{\partial z}\right) \quad (2)$$

The species mass balance in liquid (L) is expressed as follows:

$$\frac{\partial(\epsilon_{SL}C_{L,j})}{\partial t}+\frac{\partial(U_{SL}C_{L,j})}{\partial z}=-(k_La)_{SB,j}\left(C_{L,j}-\frac{C_{SB,j}}{He_j}\right)-(k_La)_{LB,j}\left(C_{L,j}-\frac{C_{LB,j}}{He_j}\right)+\frac{\partial}{\partial z}\left(\epsilon_{SL}E_{SL}\frac{\partial C_{L,j}}{\partial z}\right)-k_{S,j}a_S(C_{L,j}-C_{S,j}) \quad (3)$$

The species mass balance on the surface of solids (S) is given by eq 4. In eqs 1−4, the subscript j represents the jth species of the chemical reaction. Chemical

$$k_{S,j}a_S(C_{L,j} - C_{S,j}) + \epsilon_{SL}\nu_j k_R C_{S,1} = 0 \quad (4)$$

reaction occurs only on the surface of the solids and is assumed to be first-order with respect to the reference reactant concentration on the surface of the solids, $C_{S,1}$. Thus,

$$\sum_{j=1}^{n} \nu_j A_j = 0 \quad (5)$$

For reactants, $\nu_j < 0$, and for products, $\nu_j > 0$.

In this work, the solids axial distribution is assumed to be uniform. However, the addition of the SDM model equation to account for nonuniform distribution is both possible and straightforward because the SDM equation is only weakly coupled with the rest of the model equations. Given the particle size of below 50 μm that is usually encountered in industrial slurry systems, the intraparticle temperature and concentration profiles are most often negligible. Therefore, the solids intraparticle mass- and heat-transfer resistances are neglected.

Equation 4 for the solids-phase species mass balance is solved for the solids surface concentration, which is then substituted into the liquid-phase species mass balance (eq 3). The species mass balance in the liquid (slurry compartment) is considered for all of the n chemical species. Species mass balance equations in SB and LB compartments (eqs 1 and 2) are expressed for $n - 1$ species. The concentrations of the remaining species in these compartments are calculated from the overall momentum balance equation:

$$C_G = \sum_{j=1}^{n} C_{SB,j} = \sum_{j=1}^{n} C_{LB,j} = \frac{P + \epsilon_{SL}\rho_{SL}g(H_D - z)}{RT} \quad (6)$$

The local pressure is calculated as the summation of the reactor inlet pressure and the static head pressure.

The change in the gas flow rate is calculated from the overall gas mass balance equation that includes both SB and LB:

$$\frac{\partial(\epsilon_G C_G)}{\partial t} + \frac{\partial(U_G C_G)}{\partial z} = -\sum_{j=1}^{n}(k_L a)_{SB,j}\left(\frac{C_{SB,j}}{He_j} - C_{L,j}\right) - \sum_{j=1}^{n}(k_L a)_{LB,j}\left(\frac{C_{LB,j}}{He_j} - C_{L,j}\right) \quad (7)$$

The total gas holdup and the holdups and velocities of the two bubble classes (SB and LB) are dependent on the superficial gas velocity (SGV) and the physical properties of the system. Therefore, they are treated as time and space (axial) dependent. Holdups and velocities of the two bubble classes are calculated using the two-bubble-class hydrodynamic model of Krishna and Ellenberger,[27] which is summarized in Table 1.

Two-bubble-class models add more physics to the modeled representation of the gas flow. The assumption that all of the gas volume is present only in the form of small bubbles may lead (when the process is gas−liquid mass-transfer controlled) to the overestimation of conversion, because of the much larger area that is available for the gas−liquid mass transfer. However, if one accounts for the two bubble classes but does not account for the bubble−bubble interactions (CF in the present model), the calculated conversion may be lower than the actual. The large amount of gas that is present in LB in this case practically bypasses the reactor because the unit volume area available for the LB−liquid (L) mass transfer is much lower than that for the SB−L mass transfer.

Table 1. Hydrodynamic Model[a,27]

$\epsilon_{TR} = 0.994\sqrt{B^3\frac{\rho_G}{\rho_L}V_{SB}}$	
$V_{SB} = \frac{1}{2.84}\frac{\sigma_L^{0.12}}{\rho_G^{0.04}}$	$U_{TR} = V_{SB}\epsilon_{TR}(1 - \epsilon_{TR})$
$\epsilon_{LB} = 0.268\frac{(U_G - U_{TR})^{0.58}}{D^{0.18}}$	$U_{LB} = U_G - U_{SB}$
$\epsilon_{SB} = \epsilon_G - \epsilon_{LB}$ $\epsilon_G = \epsilon_{LB} + \epsilon_{TR}(1 - \epsilon_{LB})$	$U_{SB} = V_{SB}\epsilon_{SB}$
$\frac{\partial\epsilon_{LB}}{\partial\xi} = \Omega\frac{\partial U_G}{\partial\xi}$	$\frac{\partial U_{LB}}{\partial\xi} = (1 + V_{SB}\epsilon_{TR}\Omega)\frac{\partial U_G}{\partial\xi}$
$\frac{\partial\epsilon_{SB}}{\partial\xi} = -\epsilon_{TR}\Omega\frac{\partial U_G}{\partial\xi}$	$\frac{\partial U_{SB}}{\partial\xi} = -V_{SB}\epsilon_{TR}\Omega\frac{\partial U_G}{\partial\xi}$
$\frac{\partial\epsilon_G}{\partial\xi} = (1 - \epsilon_{TR})\Omega\frac{\partial U_G}{\partial\xi}$	$\Omega = 0.155\frac{(U_G - U_{TR})^{-0.42}}{D^{0.18}}$

[a] $\xi = t$ or z.

The change in temperature is calculated from the slurry-phase energy balance.

$$\frac{\partial(\epsilon_{SL}h_{SL})}{\partial t} + \frac{\partial(U_{SL}h_{SL})}{\partial z} = -h_W a_W(T - T_W) + \frac{\partial}{\partial z}\left(\epsilon_{SL}\lambda_{SL}\frac{\partial T}{\partial z}\right) - \epsilon_{SL}\nu_1 k_R C_{S,1}(-\Delta H_R) \quad (8)$$

All liquid−solid interfacial heat-transfer resistances are neglected. The slurry phase is assumed to be in thermal equilibrium with the gas phases. Because of high-intensity mixing in churn-turbulent SBCs, these assumptions are justified. In addition, the enthalpy of phase change (evaporation/condensation) is also neglected. For example, even for a highly exothermic FT process, the error in the overall enthalpy balance from neglecting the thermal effects of the phase change is estimated at a maximum of 10−15%. This is considered small compared to, for example, the uncertainty in the prediction of gas holdup or axial dispersion coefficient using the open literature correlations. Equations 1−8 are combined with the holdup and velocity time and axial derivatives found in Table 1.

All of the terms that are not listed in the model equations are neglected because they give negligible values based on a magnitude sensitivity analysis. The CF parameter, K, has been estimated using one-dimensional cold-flow steady-state parameter analysis. On the basis of such an analysis and on the lack of a more reliable estimate, the value is kept at 5, which gives moderate extent of SB−LB interactions.

The initial conditions are consistent with the boundary conditions. SB and LB species concentrations are set to the inlet values of the gas species concentrations. Gas at the reactor inlet contains only reactants. Initially and at the reactor inlet, liquid is assumed to be saturated with the gas phase. The boundary conditions are of the Danckwerts type and are presented in Table 2.

The model yields a system of $3n$ partial differential equations (PDEs) that are solved in dimensionless

Table 2. Initial and Boundary Conditions

initial condition ($t = 0$)	reactor inlet ($z = 0$)	reactor outlet ($z = H_D$)
$C_{SB,j} = C_{G0,j}$	$\epsilon_{SB}E_{SB}(\partial C_{SB,j}/\partial z) = U_{SB}C_{SB,j} - U_{SB0}C_{G0,j}$	$\partial C_{SB,j}/\partial z = 0$
$C_{LB,j} = C_{G0,j}$	$\epsilon_{LB}E_{LB}(\partial C_{LB,j}/\partial z) = U_{LB}C_{LB,j} - U_{LB0}C_{G0,j}$	$\partial C_{LB,j}/\partial z = 0$
$C_{L,j} = C_{G0,j}/He_{0,j}$	$\epsilon_{SL}E_{SL}(\partial C_{L,j}/\partial z) = U_{SL}C_{L,j} - U_{SL}(C_{G0,j}/He_{0,j})$	$\partial C_{L,j}/\partial z = 0$
$T = T_0$	$\epsilon_{SL}\lambda_{SL}(\partial T/\partial z) = U_{SL}h_{SL} - U_{SL}h_{SL0}$	$\partial T/\partial z = 0$
$U_G = U_{G0}$	$U_G = U_{G0}$	

form[26] using the freeware collocation software PDECOL.[28] For characterizing the processes that involve expansion or contraction of the gas phase, linear kinetic rates involving two chemical species (A and P) are used, which give a system of six PDEs. However, for modeling FT synthesis,[26] four chemical species (H_2, CO, H_2O, and a pseudoproduct) were considered, which resulted in a system of 12 PDEs.

3. Simulation of Reacting Slurry Systems with Expansion or Contraction of the Gas Phase

Two chemical reaction slurry systems with first-order kinetics are used to characterize the reactor performance and experienced a change in the gas-phase volume due to the reaction. The first system is characterized by contraction of the gas phase, A → 0.5P, while the second system is characterized by expansion of the gas phase, A → 1.5P. Dimensionless groups[26] are kept constant at values calculated from the correlations given by Mills et al.[6] for the FT SBC reactor. The operating conditions and geometry of the reactor are also in accordance with those used by Mills et al.[6] The model of Rados et al.[26] is used in this work to analyze the performance for these two reacting systems under various operating conditions. Figures 2 and 3 show (a) the transient solution profiles (dimensionless SGV, temperature, and species phase concentrations) at the reactor outlet and (b) the axial solution profiles at the steady-state operation for the two studied slurry systems. Reactor operation is found to be nearly isothermal for both kinetics. This is expected because one of the advantages of SBC reactors is a good heat-transfer rate. The SGV decreases with time and along the reactor in the gas contraction kinetics case (Figure 2). The SGV increases with time and along the reactor in the gas expansion kinetics case (Figure 3). The predicted change in SGV is expected and is qualitatively in agreement with the predictions of other models (e.g., ref 6).

The concentration of the gas reactant is smaller in SB than in LB because of the larger interfacial area that is available for mass transfer between SB and L. Mass transfer of the reactant from LB into the liquid phase becomes pronounced only at relatively low concentrations of reactant in SB. This transfer either is direct LB−L mass transfer or occurs indirectly through SB−LB CF bubble interactions followed by the SB−L mass transfer. The reactant conversion

$$X_A = 1 - \frac{U_{SB}C_{SB,A} + U_{LB}C_{LB,A} + U_{SL}C_{L,A}}{U_{G0}C_{G0,A} + U_{SL}C_{L0,A}} \quad (9)$$

is lower with the expansion of gas (Figure 3) because in this case the gas velocity increases along the reactor, reducing the mean residence time. In the case of contraction kinetics, the small local minimum of the

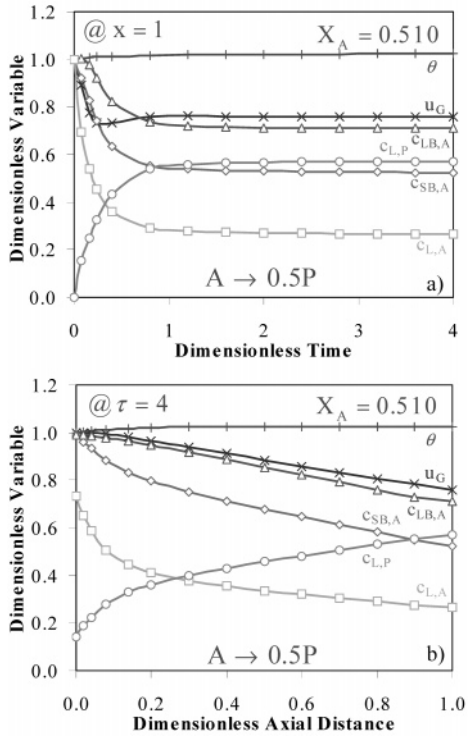

Figure 2. Time (a) and axial (b) profiles for the kinetics with gas contraction. $U_G = 0.10$ m/s, $U_{SL} = 0.02$ m/s, $H_D = 5.00$ m, and $D = 0.05$ m.

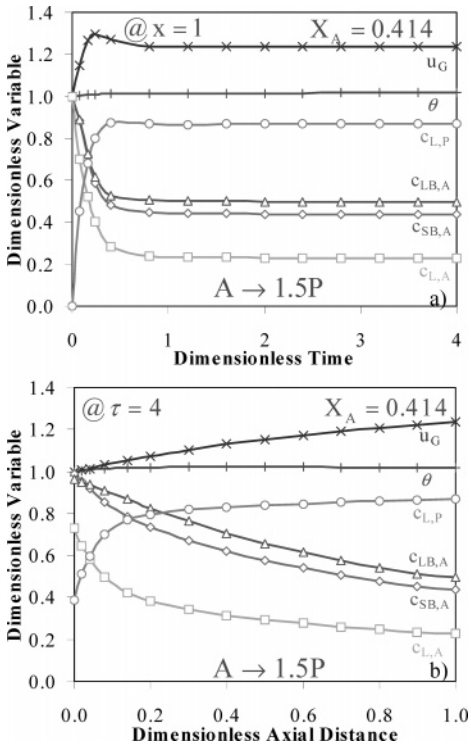

Figure 3. Time (a) and axial (b) profiles for the kinetics with gas expansion. $U_G = 0.10$ m/s, $U_{SL} = 0.02$ m/s, $H_D = 5.00$ m, and $D = 0.05$ m.

SGV transient profile is a consequence of the selected Henry's constants, i.e., solubilities ($He_A = 4$ and $He_P = 4$). Because of its relatively low Henry's constant, the product cannot transfer fast enough into the gas phase to compensate for the lost reactant from the gas phase. As can be seen from Figure 4, this minimum does not exist in cases with higher Henry's constants of the

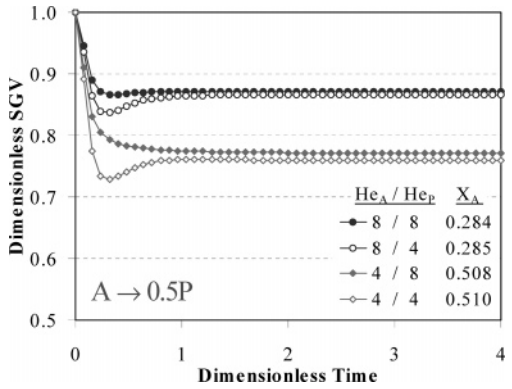

Figure 4. Effect of the reactant and product solubility on the transient SGV Profiles. $U_G = 0.10$ m/s, $U_{SL} = 0.02$ m/s, $H_D = 5.00$ m, and $D = 0.05$ m.

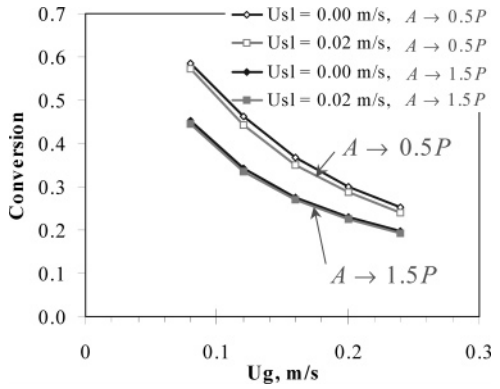

Figure 5. Effect of the gas and slurry superficial velocity on the reactant conversion. $H_D = 5.00$ m, and $D = 0.05$ m.

product ($He_A = 4$ and $He_P = 8$). If the Henry's constant of the reactant is increased ($He_A = 8$), the conversion drops because of the lower mass transfer of the reactant in the liquid phase.

The time profile of the SGV is very much dependent on the hydrodynamics and mass-transfer models used. The applied two-bubble-class model is not time-dependent, meaning that any change in the gas holdup immediately causes a change in the gas velocity. In reality, because of inertia, there will always be some time lag, causing the initial gas velocity time gradients to be lower than those calculated.

The applied mass-transfer model is based on film theory, causing the mass-transfer flux to be linearly proportional to the driving force (concentration difference). However, this is not necessarily the case when the driving force is large. Hence, an overestimated rate of mass transfer also results in steeper initial gas velocity time gradients (before the mass-transfer equilibrium is established). From Figure 4, it can be seen that a higher initial SGV time gradient causes a more pronounced local SGV minimum. The same reasoning is valid for the small local maximum of the SGV time profile in systems with expansion of the gas phase (Figure 3).

The gas conversion decreases with an increase in the gas velocity because of the decrease in the residence time of the reactants. The gas conversion also slightly decreases with an increase in the slurry velocity, but this effect is marginal compared to the effect of the gas velocity (Figure 5). As expected, the gas conversion increases with the reactor height because of the increase in the residence time and decreases with an increase

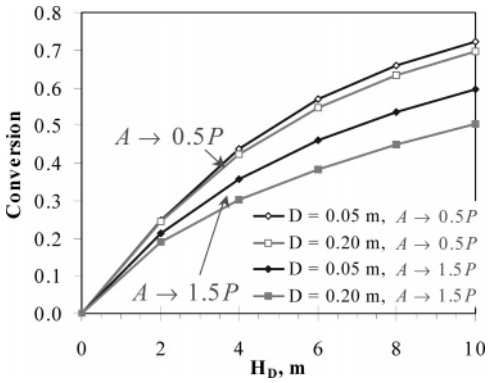

Figure 6. Effect of the reactor height and diameter on the reactant conversion. $U_G = 0.10$ m/s, and $U_{SL} = 0.02$ m/s.

in the reactor diameter because of the higher degree of axial backmixing (Figure 6). The effect of the column diameter is more pronounced in the case of gas-expanding kinetics. This is a consequence of the correlations that are used for calculating Peclet numbers.[5,6] In these correlations, Pe_G and Pe_{SL} are nonlinear functions of the column diameter and SGV. For example, Pe_G is proportional to the cube of SGV. An increase in SGV of 20% increases Pe_G by 72.8% in the expansion case, while the same decrease in SGV in the contraction case decreases Pe_G by 48.8%, an effect that is almost 1.5 times smaller.

The model of Rados et al.[26] calculates the change in SGV from the total gas mass balance. This approach is physically more justified than the widely used approach based on the linear dependency between the conversion and the gas flow rate, shown in eq 10 (e.g., ref 5).

$$U_G = U_{G0}\frac{P_0}{P}\frac{T}{T_0}(1 + \alpha X_G) \tag{10}$$

Additionally, calculation of SGV using eq 10 requires input of the contraction factor α.[25] For complex reaction kinetic schemes, α must be a priori experimentally determined. Stern et al.[24] showed that eq 10 is valid only for steady-state operation with no liquid−slurry convection and no liquid−slurry backmixing. In other words, in rare cases the only important terms in eq 3 are the gas−liquid and liquid−solid mass transfers, as given in eq 11. The total gas mass balance presented in

$$(k_L a)_{SB,j}\left(C_{L,j} - \frac{C_{SB,j}}{He_j}\right) + (k_L a)_{LB,j}\left(C_{L,j} - \frac{C_{LB,j}}{He_j}\right) = k_{S,j} a_S (C_{L,j} - C_{S,j}) \tag{11}$$

eq 7 to calculate the change in the gas flow rate indicates that such a change is affected by the gas−liquid mass transfer, which is further affected by the liquid−solid mass transfer and chemical reaction. This approach does not require a priori knowledge of the contraction factor. However, it requires calculation of the concentrations of all gaseous species and is therefore more numerically involved and computationally intensive.

SGV directly affects the mean residence time and reactor performance. Therefore, reliable calculation of a change in SGV is vital for the proper prediction of the reactor performance. The two approaches in calculating a change in SGV (eqs 7 and 10) can to some extent be indirectly compared. The SGV steady-state profile obtained using the Rados et al.[26] model can be compared

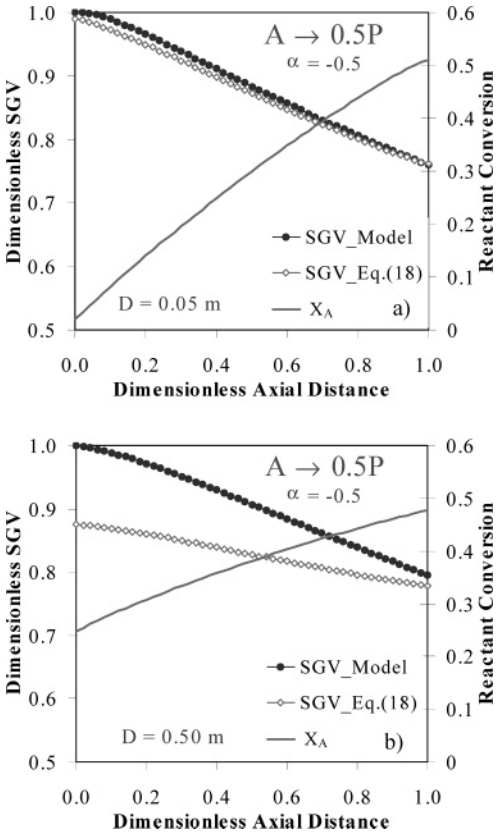

Figure 7. Comparison between steady-state SGV profiles predicted by the present model and calculated using eq 10 with the model-predicted reactant conversion profiles. $U_G = 0.10$ m/s, $U_{SL} = 0.02$ m/s, $H_D = 5.00$ m, and $D = 0.05$ m (a) or 0.50 m (b).

with the SGV profile calculated using eq 10 and the model-predicted conversion (eq 9). If the two profiles are comparable, as in Figure 7a, then the predicted steady-state SGV profiles using the Rados et al.[26] model and the linear model (eq 10) are also comparable. In the case of a small reactor diameter, backmixing is negligible and the reactor operation is close to the PF mode (Figure 7a, $D = 0.05$ m). The low slurry velocity of 0.02 m/s suggests small slurry convection effects. Because all three conditions (steady-state operation, no slurry convection, and no backmixing effects)[24] are reasonably well achieved, the SGV predictions using the two approaches are comparable. In similar manner, Figure 7b compares two SGV profiles for a 0.50-m-diameter SBC reactor. The backmixing in this reactor is much larger (Pe_{SL} is about 30 times larger), and consequently there is a noticeable discrepancy between the two SGV profiles (up to 13%, Figure 7b). From the above analysis, it is obvious that the two often used assumptions, completely mixed slurry and simplified linear dependency of SGV on conversion (eq 10), are not compatible. In industrial large-scale reactors, depending on the design parameters, backmixing can be considerable, and predictions of SGV using the simplified approach may cause significant errors.

4. Role of Backmixing on the Performance Prediction of FT Synthesis

All of the published models of the FT process have treated the solids and liquid as one pseudo-homogeneous slurry phase. The slurry phase is most often modeled as a completely mixed tank[8,12,13] or by using the ADM.[5,6,14,26] The gas phase has been traditionally modeled as a single phase, in PF or with some axial dispersion. In the past few years, several models that treat the gas phase using the two-bubble-class approach have been proposed. Using this approach, the SB phase is modeled as completely mixed (as a slurry phase), while the LB phase is modeled in the PF mode.[12,13] Alternatively, both of the gas phases are modeled using the ADM.[14,22,26] Table 3 summarizes the features included in some of the models for a FT SBC reactor.

Rados et al.[26] used hydrogen-controlled, first-order FT synthesis kinetics in their model:

$$H_2 + 0.5CO \xrightarrow{k_{FT\ synthesis}} 0.1C_5H_{10} + 0.5H_2O \quad (12)$$

All other side reactions (including water gas shift, WGS) were neglected. They presented detailed simulation results: the transient profiles at the reactor outlet and the steady-state operation axial profiles for two different inlet ratios ($I = 0.5$, hydrogen lean, and $I = 2.0$, stoichiometric syngas composition) and two different reactor diameters ($D = 0.05$ and 0.50 m). In the present work, additional analyses have been conducted using the model of Rados et al.[26] to demonstrate the role of backmixing on the prediction of the FT SBC reactor performance.

Tables 4−6 summarize the effect of backmixing on the performance predictions of FT SBC reactors with diameters of 0.05, 0.5, and 2.0 m, respectively. The performance predictions using the Rados et al.[26] compartmental model (SB, LB, and SL compartments or phases are modeled using ADM) are compared with the performance predictions obtained using several combinations of ideal reactor models for these compartments in which the phase backmixing is assumed to be either complete (CST mode) or negligible (PF mode). PF and CST modes are simulated by setting the value of the axial dispersion coefficient in the model of Rados et al.[26] to 0 and ∞, respectively. Because the 0.05-m-diameter reactor exhibits small backmixing, the full PF model (full PF means all compartments are modeled using PF) matches well the conversion obtained using the full ADM model (error < 1%), while the other combinations of ideal reactor models mismatch the conversion with error > 8%. For the intermediate 0.50-m-diameter reactor, the full PF model and the reactor with G-PF and SL-CST models approach the full ADM model within 5% (Table 5). For the 2.0-m-diameter reactor, which had the lowest aspect ratio and the largest extent of backmixing of all of the reactor sizes used, the G-PF, SL-CST, LB-PF, SB-CST, and SL-CST models approach the full ADM model conversion within 5% (Table 6). Obviously, the conversion of the full ADM model can be fairly matched with some combinations of the ideal reactor modes. However, the best combination of the ideal reactor modes depends on the reactor diameter, i.e., on the extent of actual backmixing. Thus, one would need to a priori estimate the extent of backmixing based on the column diameter and other parameters. The often used full CST model is about 7% off in matching the conversion of the full ADM model, even in the 2.0-m-diameter reactor. For all considered reactor diameters (0.05, 0.50, and 2.0 m and larger), the mismatch in the predicted conversions using full PF models (SB, LB, and SL in the PF mode) and full CST models (SB, LB, and SL in the CST mode) is about 20%. For this set of operating and inlet conditions, 20% is also the maximum

Table 3. Summary of Some of the FT SBC Reactor Models

model	kinetics	species	phase degree of mixing	gas velocity profile	solids profile	energy balance	steady-state model
Rados et al.[26]	FTS, 1st	H_2, CO, CO_2, product	SB, LB, SL-ADM	computed	uniform	yes	dynamic
de Swart and Krishna[22]	FTS, 1st	H_2	SB-CST or PF, LB-PF, SL-CST	linear $f(X,\alpha)$	SDM	yes	dynamic
van der Laan et al.[13]	FTS, L−H WGS, L−H	H_2, CO H_2O, CO_2 *n* products	SB-CST LB-PF SL-CST	linear $f(X,\alpha)$	uniform	yes	yes
Maretto and Krishna[12]	FTS, L-H	H_2, CO	SB-CST, LB-PF, SL-CST	uniform	uniform	isothermal	yes
Mills et al.[6]	FTS, 1st	H_2	G-ADM, SL-ADM	linear $f(X,\alpha)$	SDM	yes	yes
Leib et al.[21]	FTS, 1st	H_2	G-MCM, L-MCM	linear $f(X,\alpha)$	uniform	isothermal	yes
Prakash[23]	FTS, L−H WGS, L−H	H_2, CO, H_2O, CO_2	G-ADM SL-ADM	overall gas MB	SDM	yes	yes
Turner and Mills[29]	FTS, 1st	H_2	G-MCM, L-MCM, G-ADM, L-ADM	linear $f(X,\alpha)$	SDM	yes	yes
Kuo[30]	FTS, L−H WGS, L−H	H_2, CO, H_2O, CO_2	G-PF SL-PF, CST or ADM	linear $f(X,\alpha)$	uniform	isothermal	yes
Stern et al.[24]	FTS, 1st WGS, 2nd	H_2, CO H_2O, CO_2, C_nH_m	G-ADM SL-ADM	overall gas MB	SDM	isothermal	yes
Bukur[8]	FTS, 1st	H_2	G-PF, SL-CST	linear $f(X,\alpha)$	uniform	isothermal	yes
Deckwer et al.[5]	FTS, 1st	H_2	G-ADM, SL-ADM	linear $f(X,\alpha)$	SDM	isothermal	yes

[a] 1st = first order, 2nd = second order, L−H = Langmuir−Hinshelwood reaction kinetics.

Table 4. Effect of the Backmixing Extent for the 0.05-m-Diameter Reactor[a]

run no.	SB	LB	SL	X_{H_2}	error, %
1	CST	CST	CST	0.445	−17.7
2	CST	PF	CST	0.454	−16.1
3	PF	PF	CST	0.496	−8.3
4	**ADM**	**ADM**	**ADM**	**0.541**	
5	PF	PF	PF	0.542	+0.2

[a] $I = 2.0$, $U_G = 0.10$ m/s, $U_{SL} = 0.02$ m/s, and $H_D = 5.00$ m.

Table 5. Effect of the Backmixing Extent for the 0.50-m-Diameter Reactor[a]

run no.	SB	LB	SL	X_{H_2}	error, %
1	CST	CST	CST	0.450	−14.6
2	CST	PF	CST	0.461	−12.5
3	PF	PF	CST	0.503	−4.6
4	**ADM**	**ADM**	**ADM**	**0.527**	
5	PF	PF	PF	0.554	+5.1

[a] $I = 2.0$, $U_G = 0.10$ m/s, $U_{SL} = 0.02$ m/s, and $H_D = 5.00$ m.

Table 6. Effect of the Backmixing Extent for the 2.0-m-Diameter Reactor[a]

run no.	SB	LB	SL	X_{H2}	error, %
1	CST	CST	CST	0.454	−6.8
2	CST	PF	CST	0.466	−4.3
3	**ADM**	**ADM**	**ADM**	**0.487**	
4	PF	PF	CST	0.509	+4.5
5	PF	PF	PF	0.560	+15.0

[a] $I = 2.0$, $U_G = 0.10$ m/s, $U_{SL} = 0.02$ m/s, and $H_D = 5.00$ m.

possible error in predicting conversion when the ideal reactor modes for different phases are not well selected.

However, the maximum error in the predicted conversion could be larger than 20% if the considered reaction order is larger than 1. This is because an increase in the reaction order increases conversion in the fully PF reactor and decreases conversion in the fully CST reactor. In the present FT SBC reactor case study, first-order kinetics is assumed. This assumption is shown to be valid when hydrogen conversion is below 60%,[31] as in the present study. When conversion increases above 60%, the adsorption term of the Langmuir−Hinshelwood kinetics becomes increasingly important, and hence the order of the reaction with respect to carbon monoxide is no longer 0, and the overall order of the reaction becomes larger than 1. Hence, the assumption that the FT reaction order is 1 does not hold at conversions above 60%, and additionally, it increases the mismatch in the predicted conversion to more than 20%, when the ideal reactor modes for the three phases are not properly selected.

Unfortunately, just matching the conversion is not a proof that the two models with different combinations of backmixing modes predict the same concentration profiles. For example, in the case of the 0.50-m-diameter reactor, although the full ADM model conversion is matched within 5% using the full PF model, the steady-state axial concentration profiles are quite different for the two models (compare Figure 8b of this study with Figure 4 from Rados et al.[26]). Moreover, the ADM-predicted concentration profiles are definitely not completely invariant with the axial distance, as the full CST model predicts (Figure 8a).

Although Tables 4−6 show that the full ADM model is more versatile than the ideal reactor modeling approach, it is known that proper predictions of ADM rely on the accuracy of the correlations used for Peclet number calculations in different phases. Often these correlations are not accurate or are not existent, which makes the predictions of the ADM model questionable. In this case, the ideal reactor model consisting of G-PF and SL-CST (or G-PF and SL-PF for very slender reactors) or the tank-in-series model would be considered.

5. Summary

The dynamic and compartmental-based SBC reactor-scale model of Rados et al.[26] has been utilized to assess the reactor performance when the gas volume changes along the reactor (i.e., contraction or expansion). The change in the gas flow rate caused by the chemical reaction is calculated using the overall gas mass balance, where all of the relevant gaseous chemical species are accounted for. This approach is shown to be more realistic and appropriate than the commonly used approach based on the linear relationship between the conversion and SGV.

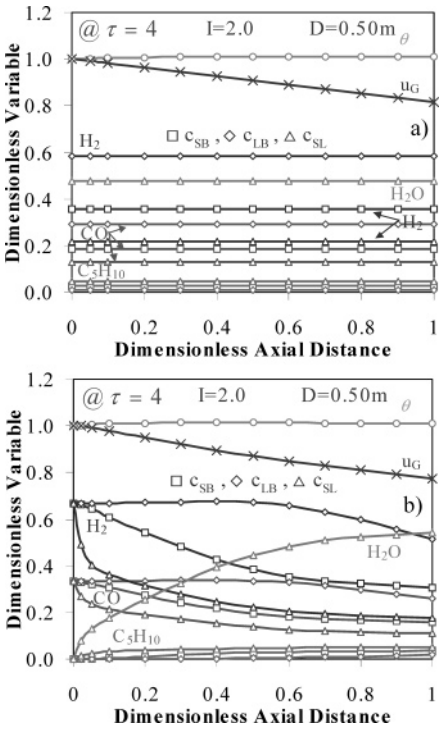

Figure 8. FT steady-state axial profiles using the full CST model (a, $X_{H_2} = 0.450$) and full PF model (b, $X_{H_2} = 0.554$). $I = 2.0$, $U_G = 0.10$ m/s, $U_{SL} = 0.02$ m/s, $H_D = 5.00$ m, and $D = 0.50$ m.

The model predictions have been demonstrated using general first-order kinetics in SBC reactors with expansion and contraction of the gas phase. Additionally, the effect of backmixing on the performance of various FT SBC reactor sizes has been analyzed and discussed. Significant differences in the model predictions for SBC reactors of the three different diameters used have been found when a change in the gas flow rate has not been properly modeled and/or when the axial dispersion has not been properly accounted for. These differences are expected to be larger in cases when the reaction order is higher than 1.

Utilization of the full ADM approach to model the backmixing in the three compartments of the model is shown to be more versatile than the approach using a combination of the two ideal reactor modes (PF and CST). If the Peclet number correlations are inaccurate or are not existent, modeling of the gas phase should be attempted in the PF mode. The slurry phase could be considered either in the PF mode for narrow reactors, in the CST mode for large-diameter reactors, or in the general case as several CST compartments in series. The ideal reactor-scale model in which all three phases are in the CST mode (i.e., full CST model) should be avoided. Compared to the predictions of the full ADM model, the full CST model underpredicts the conversion, even for the large-diameter reactors (2.0 m and larger).

Notation

a_W = cooling surface unit volume area, m_W^2/m_{SL}^3
B = Reilly's constant: 3.84
c = dimensionless concentration: C/C_{G0}
C = concentration, mol/m^3
D = reactor diameter, m
E = axial dispersion coefficient, m^2/s
g = gravity: 9.80 m/s^2
h = enthalpy, J/m^3
H_D = reactor dynamic height, m
He = Henry's solubility constant, m_{SL}^3/m_G^3
ΔH_R = reaction heat, J/mol
h_W = cooling surface convective heat-transfer coefficient, $J/m^2 \cdot K \cdot s$
I = FT reactor inlet ratio: $c_{H_2,0}/c_{CO,0}$
k = chemical reaction rate coefficient, 1/s
K = bubble−bubble dimensionless interaction cross-flow coefficient
k_La = mass-transfer coefficient, 1/s
n = total number of chemical species considered in a modeled chemical process
N = number of continuously stirred tanks in the cascade (MCM model)
P = pressure, Pa
Pe_i = Peclet number of the phase i: $U_{i,0}H_D/E_i$
R = ideal gas constant: 8.314 J/mol·K
t = time, s
T = temperature, K
u = dimensionless superficial velocity: U/U_{G0}
U = superficial velocity, m/s
V = bubble rise velocity, m/s
x = dimensionless axial position: z/H_D
X_j = conversion of the species j
z = axial position, m

Greek Letters

α = contraction factor
ϵ = phase holdup, $m_{phase}^3/m_{reactor}^3$
λ = heat conductivity, J/m·K·s
ν_j = stoichiometric coefficient of the jth species
ρ = density, kg/m^3
σ = surface tension, kg/m·s
τ = dimensionless time: tU_{G0}/H_C
Ω = parameter defined in Table 1

Subscripts

0 = inlet of the reactor
1 = reference reactant
G = gas phase
i = phase denominator
j = chemical species denominator
L = liquid phase
LB = large bubbles
S = solids
SB = small bubbles
SL = slurry phase
TR = gas at the point of bubbly to churn-turbulent flow transition
W = wall

Literature Cited

(1) Deckwer, W.-D.; Alper, E. Katalytische Suspensions Reaktoren. *Chem. Eng. Tech*. **1980**, *52*, 219.

(2) Shah, Y. T.; Kelkar, B. G.; Godbole, S. P.; Deckwer, W.-D. Design Parameter Estimation for Bubble Column Reactors. *AIChE J.* **1982**, *28*, 353.

(3) Dry, M. E. The SASOL Route to Fuels. *CHEMTECH* **1982**, *12*, 744.

(4) Kato, Y.; Nishiwaki, T.; Fukuda, T.; Tanaka, S. The Behavior of Suspended Solid Particles and Liquid in Bubble Columns. *J. Chem. Eng. Jpn.* **1972**, *5*, 112.

(5) Deckwer, W.-D.; Serpemen, Y.; Ralek, M.; Schmidt, B. Modeling of the Fischer−Tropsch Synthesis in the Slurry Phase. *Ind. Eng. Chem. Process Des. Dev.* **1982**, *21,* 231.

(6) Mills, P. L.; Turner, J. R.; Ramachandran, P. A.; Dudukovic, M. P. The Fischer−Tropsch Synthesis in Slurry Bubble Column Reactors: Analysis of Reactor Performance Using the Axial Dispersion Model. *Topics in Chemical Engineering*; Gordon & Breach Science Publishers: New York, 1996; Vol. 8.

(7) Murray, P.; Fan, L.-S. Axial Solid Distribution in Slurry Bubble Columns. *Ind. Eng. Chem. Res.* **1989**, *28*, 1697.

(8) Bukur, D. B. Models for Fischer−Tropsch Reaction in Slurry Bubble Column Reactors. *Chem. Eng. Sci.* **1983**, *38*, 441.

(9) Bukur, D. B.; Kumar, V. R. Effect of Catalyst Dispersion on Performance of Slurry Bubble Column Reactors. *Chem. Eng. Sci.* **1986**, *41*, 1435.

(10) Sriram, K.; Mann, R. Dynamic Gas Disengagement: A New Technique for Assessing the Behavior of Bubble Columns. *Chem. Eng. Sci.* **1977**, *32*, 571.

(11) Varmeer, D. J.; Krishna, R. Hydrodynamics and Mass Transfer in Bubble Columns Operating in the Churn-Turbulent Regime. *Ind. Eng. Chem. Process Des. Dev.* **1981**, *20*, 475.

(12) Maretto, C.; Krishna, R. Modeling of a Bubble Column Slurry Reactor for Fischer−Tropsch Synthesis. *Catal. Today* **1999**, *52*, 279.

(13) van der Laan, G. P.; Beenackers, A. A. C. M.; Krishna, R. Multicomponent Reaction Engineering Model for Fe-catalyzed Fischer−Tropsch Synthesis in Commercial Scale Slurry Bubble Column Reactors. *Chem. Eng. Sci.* **1999**, *54*, 5013.

(14) de Swart, J. W. A. Scale-up of a Fischer−Tropsch Slurry Reactor. Ph.D. Thesis, University of Amsterdam, Amsterdam, The Netherlands. 1996.

(15) Shah, Y. T.; Joseph, S.; Smith, D. N.; Ruether, J. A. Two-Bubble Class Model for Churn-Turbulent Bubble-Column Reactor. *Ind. Eng. Chem. Process Des. Dev.* **1985**, *24*, 1096.

(16) Modak, S. Y.; Juvekar, V. A.; Rane, V. C. Comparison of the Single-Bubble-Class and Modified Two-Bubble-Class Models of Bubble Column Reactors. *Chem. Eng. Technol.* **1994**, *17*, 313.

(17) Kantak, M. V.; Hesketh, R. P.; Kelkar, B. G. Effect of Gas and Liquid Properties on Gas-Phase Dispersion in Bubble Columns. *Chem. Eng. J.* **1995**, *59*, 91.

(18) Hartland, S.; Mecklenburgh, J. C. A Comparison of Differential and Stagewise Counter Current Extraction with Backmixing. *Chem. Eng. Sci.* **1966**, *21*, 1209.

(19) Chianese, A. A Mathematical Model of a Bubble Column Reactor for the Cumene Oxidation. *Chem. Eng. Commun.* **1982**, *17*, 261.

(20) Schluter, S.; Steiff, A.; Weinspach, P.-M. Modeling and Simulation of Bubble Column Reactors. *Chem. Eng. Process* **1992**, *31*, 97.

(21) Leib, T. M.; Mills, P. L.; Lerou, J. J.; Turner, J. R. Evaluation of Neural Networks for Simulation of Three-Phase Bubble Column Reactors. *Chem. Eng. Res. Des.* **1995**, *73* (A6), 690.

(22) de Swart, J. W. A.; Krishna, R. Simulation of the Transient and Steady-State Behavior of a Bubble Column Slurry Reactor for Fischer−Tropsch Synthesis. *Chem. Eng. Process* **2002**, *41*, 35.

(23) Prakash, A. On the Effect of Syngas Composition and Water-Gas-Shift Reaction Rate on FT Synthesis over Iron Based Catalyst in a Slurry Reactor. *Chem. Eng. Commun.* **1993**, *128*, 143.

(24) Stern, D.; Bell, A. T.; Heinemann, H. A Theoretical Model for the Performance of Bubble-Column Reactors Used for Fischer−Tropsch Synthesis. *Chem. Eng. Sci.* **1985**, *40,* 1665.

(25) Levenspiel, O. *Chemical Reaction Engineering*, 2nd ed.; John Wiley & Sons: New York, 1972.

(26) Rados, N.; Al-Dahhan, M.; Dudukovic, M. P. Modeling of the Fischer Tropsch Síntesis in Slurry Bubble Column Reactors. *Catal. Today* **2003**, *79*−*80*, 211−218.

(27) Krishna, R.; Ellenberger, J. Gas Holdup in Bubble Column Reactors Operating in the Churn Turbulent Flow Regime. *AIChE J.* **1996**, *42*, 2627.

(28) Sincovec, R. F.; Madsen, N. K. Software for Nonlinear Partial Differential Equations. *Acm-Toms* **1975**, *1*, 232.

(29) Turner, J. R.; Mills, P. L. Comparison of Axial Dispersion and Mixing Cell Models for Design and Simulation of Fischer−Tropsch Slurry Bubble Column Reactors. *Chem. Eng. Sci.* **1990**, *45*, 2317.

(30) Kuo, J. C. W. *Slurry Fischer−Tropsch/Mobil Two-Stage Process of Converting Syngas to High Octane Gasoline*; Final Report DOE/PC/30022-10; U.S. DOE: Washington, DC, 1983.

(31) Huff, G. A., Jr.; Satterfield, C. N. Intrinsic Kinetics of the Fischer−Tropsch Synthesis on a Reduced Fused-Magnetite Catalyst. *Ind. Eng. Chem. Process Des. Dev.* **1984**, *23*, 696.

Received for review August 31, 2004
Revised manuscript received March 4, 2005
Accepted April 4, 2005

IE040227T